CRREL
REPORT 80-24

Measurement of the shear stress on the underside of simulated ice covers

CRREL Report 80-24

Measurement of the shear stress on the underside of simulated ice covers

Darryl J. Calkins and Andreas Müller

October 1980

Prepared for
DIRECTORATE OF CIVIL WORKS
OFFICE OF THE CHIEF OF ENGINEERS
By
UNITED STATES ARMY
CORPS OF ENGINEERS
COLD REGIONS RESEARCH AND ENGINEERING LABORATORY
HANOVER, NEW HAMPSHIRE, U.S.A.

Unclassified

SECURITY CLASSIFICATION OF THIS PAGE *(When Data Entered)*

REPORT DOCUMENTATION PAGE

READ INSTRUCTIONS BEFORE COMPLETING FORM

1. REPORT NUMBER: CRREL Report 80-24

2. GOVT ACCESSION NO.

3. RECIPIENT'S CATALOG NUMBER

4. TITLE *(and Subtitle)*: MEASUREMENT OF THE SHEAR STRESS ON THE UNDERSIDE OF SIMULATED ICE COVERS

5. TYPE OF REPORT & PERIOD COVERED

6. PERFORMING ORG. REPORT NUMBER

7. AUTHOR(s): Darryl J. Calkins and Andreas Müller

8. CONTRACT OR GRANT NUMBER(s)

9. PERFORMING ORGANIZATION NAME AND ADDRESS: U.S. Army Cold Regions Research and Engineering Laboratory, Hanover, New Hampshire 03755

10. PROGRAM ELEMENT, PROJECT, TASK AREA & WORK UNIT NUMBERS: CWIS 31357

11. CONTROLLING OFFICE NAME AND ADDRESS: Directorate of Civil Works, Office of the Chief of Engineers, Washington, D.C. 20314

12. REPORT DATE: October 1980

13. NUMBER OF PAGES: 15

14. MONITORING AGENCY NAME & ADDRESS *(if different from Controlling Office)*

15. SECURITY CLASS. *(of this report)*: Unclassified

15a. DECLASSIFICATION/DOWNGRADING SCHEDULE

16. DISTRIBUTION STATEMENT *(of this Report)*

Approved for public release; distribution unlimited.

17. DISTRIBUTION STATEMENT *(of the abstract entered in Block 20, if different from Report)*

18. SUPPLEMENTARY NOTES

19. KEY WORDS *(Continue on reverse side if necessary and identify by block number)*

Hydraulics
Ice
Models
Roughness
Shear stresses
Simulation
Velocity
Water

20. ABSTRACT *(Continue on reverse side if necessary and identify by block number)*

The fluid shear stress applied to the underside of a simulated floating ice cover was measured in a laboratory flume. The measured values were compared with values of the shear stress computed from the von Karman-Prandtl velocity distribution fitted to the velocity profiles measured beneath the cover. For the lower velocity runs (~0.079 m/s) the measured and computed values of the shear stress were in close agreement. At the high velocity flows (~0.137 m/s) the measured values were roughly one-half those calculated from the velocity distribution. As the underside of the cover became increasingly rougher, the position of maximum velocity moved closer to the bottom of the channel. It was shown that the Darcy friction coefficient is exponentially related to a normalized ice cover thickness, which suggests that it is measure of the roughness of a fragmented ice cover.

DD FORM 1 JAN 73 1473 EDITION OF 1 NOV 65 IS OBSOLETE

Unclassified

SECURITY CLASSIFICATION OF THIS PAGE *(When Data Entered)*

PREFACE

This report was prepared by Darryl J. Calkins, Research Hydraulic Engineer, of the Ice Engineering Research Branch, Experimental Engineering Division, U.S. Army Cold Regions Research and Engineering Laboratory, and by Dr. Andreas Müller of the Institute of Hydromechanics and Water Resources, Zürich, Switzerland. Funding for this research was provided by U.S. Army Corps of Engineers Civil Works Project CWIS 31357, *Model Studies of Ice Jam Formation.*

Dr. George Ashton and James Wuebben of CRREL and Dr. Spyros Beltoas of the Research Council of Alberta, Canada, technically reviewed the manuscript of this report.

The authors appreciate the use of the facilities at the Iowa Institute of Hydraulic Research and the support given there by shop personnel, and staff members Dr. Enzo Macagno and Dr. Jean-Claude Tatinclaux.

CONTENTS

ILLUSTRATIONS

TABLES

LIST OF SYMBOLS

B	width of frame
C_d	drag coefficient on a submerged body
f_{ii}	Darcy's friction factor calculated using mean velocity V_i
f_{im}	Darcy's friction factor calculated using mean velocity $\overline{V}_m$
F_H	hydrodynamic or form drag on leading edge
F_I	force in downstream direction due to the floating ice mass
F_M	total force measured by transducers
F_S	shear force on ice cover underside
L	length of ice accumulation
n_{ice}	Manning's coefficient for roughness of the ice cover
p	porosity of the ice cover (water void/total volume)
R_e	Reynolds number
t	thickness of ice
u_i^*	shear velocity = $\sqrt{\tau_i/\rho_f}$
ν	kinematic viscosity of water
$\overline{V}_L$	mean velocity in the section influenced by the ice cover
$\overline{V}_m$	mean velocity in channel
W	weight of the cover in newtons
y_m	distance to position of maximum velocity from the ice cover underside
y_n	depth of flow, measured from ice underside to bed
y_t	total depth of water = $y_n+(\rho_i/\rho_f)$
α	frame displacement angle $<< 1^\circ$
β	slope angle of water surface
ρ_f	density of fluid
ρ_i	density of ice
τ_i	shear stress on ice cover underside
τ_{ic}	calculated shear stress on ice cover underside
τ_{im}	measured shear stress on ice cover underside

MEASUREMENT OF THE SHEAR STRESS ON THE UNDERSIDE OF SIMULATED ICE COVERS

Darryl J. Calkins and Andreas Müller

INTRODUCTION

The major driving force exerted on an ice jam is often the fluid shear transmitted to the underside of the ice cover. Pariset et al. (1966) assumed that the ice cover shear stress was equivalent to the bed shear stress in the development of their ice cover formation and evolution model.

There have been many attempts to calculate a coefficient of roughness for the underside of an ice cover, both from laboratory and field observations (Nezhikhovskiy 1964, Ashton et al. 1970, Carey 1966 and 1967, Tatinclaux and Cheng 1978, Ohashi and Hanad 1970, Tesaker 1970, Ismail 1972). The greatest difficulty lies in measuring the physical dimensions of the underside roughness element of the ice as it relates to a coefficient of friction.

The objective of the research described in this report was to experimentally measure the drag force and hence the shear stress on the underside of simulated ice covers in a laboratory flume using square polyethylene blocks of 3.18-mm thickness. Velocity profiles were measured beneath the fragmented cover, and the shear stress was calculated from these profiles and compared against the measured values.

EXPERIMENTAL APPARATUS

The experimental work was carried out at the Iowa Institute of Hydraulic Research in a 12.2-m-long, 0.61 m-wide, and 0.3-m-deep tilting flume, maintained practically horizontally for all tests. A 0.57-m-wide and 2.44-m-long wooden frame (Fig. 1), constructed from conventional 2 X 4 lumber, was suspended 3.05 m from the ceiling. A wire screen of 12.7-mm mesh was stapled around the outer surface of the frame, excluding the upstream end, and extended approximately 0.1 m below its base. The frame was designed so that the mesh would not come in contact with the flume walls.

Frame displacement was measured by strain gauge force transducers with a maximum displacement of 0.06 mm. The two transducers were connected individually by thin nylon line to the outside members of the frame at the upstream section. Initially the transducers were calibrated individually, but the nylon line stretched so that the system as a whole had to be calibrated. Output from the transducers went to a strip chart recorder. The force F_F in the streamwise direction due to the weight of the frame was incorporated into the calibration and its magnitude can be neglected.

The water velocity profiles were obtained from a Nova-Nixon small propeller current meter. The fragmented ice cover was simulated by 3.14-mm-thick X 31.7- X 38.1-mm polyethylene high density plastic blocks of 0.92 specific gravity.

EXPERIMENTAL PROCEDURES

A constant water level of 0.152 m was maintained for all experiments and after some preliminary tests two flow velocities were predominantly used, 0.082 and 0.13 m/s. The critical velocity for submergence of an individual block was calculated to be approximately 0.13 m/s based on data from Larsen (1975) and Tatinclaux et al. (1977).

When the desired flow velocity was obtained in the flume, the nylon lines between the transducers and frame were brought into tension by moving the pair of transducers in an upstream direction until a small force registered on the recorder was zeroed out. Ice was introduced into the channel near the headbox from a chute angled from the support rails to the water sur-

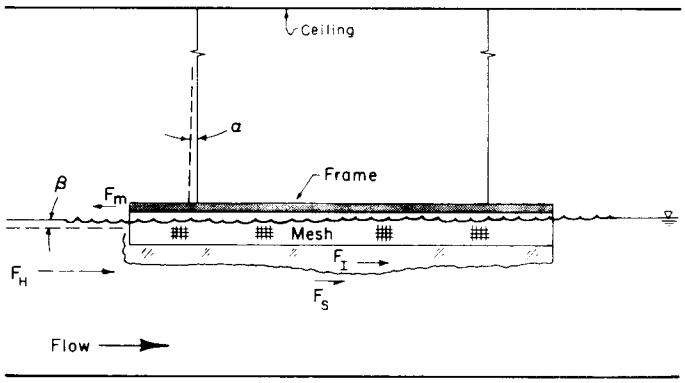

Figure 1. Experimental setup in flume.

surface. When the ice dropped into the fow, surface waves were propagated downstream, setting up temporary oscillations in the frame as indicated by the recorder output.

The total force acting on the ice mass used for calculations was determined when the system had stabilized and a constant reading attained. Velocity profiles were measured 0.76 m upstream from the downstream edge of the ice accumulation. The weight of ice discharged into the flume, length of accumulation and average thickness were also measured. The mean velocity $\overline{V}_m$ in the channel was calculated from the discharge measurements obtained with an in-line orifice plate.

ANALYSIS OF FORCES

The ice-collecting frame was designed to exclude the friction force that could be developed on the walls of the flume by ice pieces. The total force F_M measured by the transducers in the direction of flow consisted of three components: 1) hydrodynamic or form drag F_H on the leading edge, 2) shear force F_S due to the moving fluid beneath the cover including form drag of the ice blocks, and 3) weight of the ice mass F_I. Figure 1 shows a schematic view of the frame and the forces acting on the system.

The forces are:

$$F_M = F_H + F_S + F_I \qquad (1)$$

where $F_H = \frac{1}{2}\rho_f C_d t B \overline{V}_m^2$ (hydrodynamic force)
$F_S = \tau_i L B$ (shear force)
$F_I = W_I \sin\beta$ (cover force)
ρ_f = density of fluid
C_d = drag coefficient = 1.0
t = thickness of ice
B = width of frame
L = length of ice accumulation
$\overline{V}_m$ = mean fluid velocity
τ_i = shear stress on the ice cover underside

The slope of the water surface gradient was approximately 5×10^{-5} m/m, and the force F_I in the downstream direction due to an ice cover was small (< 1 mN) and consequently could be excluded. It will be shown in the experimental data section that the hydrodynamic force F_H is small compared to the measured total forces except possibly for short cover lengths. Therefore, the total force recorded by the transducer consisted primarily of the shear stress transferred to the cover's underside.

The calculation of the shear stress on the ice cover's underside was based on the projected planar area of the cover within the ice frame, such that

$$\tau_{im} = F_M / LB \qquad (2)$$

where the subscript m refers to the measured value.

The measured shear stress was compared with sheer stress calculated from the velocity profile on the assumption that the logarithmic velocity distribution could be applied to a flow depth only a few times the size of the roughness scale. A further assumption was made that the flow cross section under the ice cover could be divided into two zones from the plane of maximum velocity: 1) the ice zone and 2) the bed zone. Based on this division of areas, the logarithmic velocity distribution was applied to each section individually. The only difficulty lay in assessing the position of the upper boundary since the fragmented cover had such a variable thickness.

EXPERIMENTAL RESULTS

An initial set of experiments was conducted to determine the necessary cover length that would ensure a proper boundary layer development and to in-

Table 1. Initial shear stress tests.

Run	Length of ice cover L (m)	Weight of cover W (N)	Thickness of cover t (mm)	Total force F_M (mN)	Mean velocity $\bar{V}_m$ (m/s)	Measured shear stress τ_{im} (N/m²)	Normalized thickness t/y_n	Friction factor f_{im}	Note
S1	0.61	8.89	3.18	34.2	0.119	0.0948	–	–	
S2	1.22	13.34	3.18	46.7	0.119	0.0868	–	–	
S3	1.83	26.69	3.18	83.6	0.119	0.0773	–	–	
S4	2.44	35.59	3.18	106.3	0.119	0.0737	–	–	
S5	1.58	35.59	(13.3)	99.2	0.082	0.1058	0.095	0.1259	1
S6	1.92	48.93	(15.1)	124.1	0.082	0.1092	0.110	0.1299	1
S7	2.38	62.28	(15.5)	152.1	0.082	0.1082	0.114	0.1287	1
S8	2.44	35.59	3.18	233.5	0.137	0.1618	–	–	
S9	2.44	35.59	3.18	193.5	0.137	0.1341	–	–	4
S10	2.44	35.59	3.18	164.1	0.137	0.1140	–	–	5
S11	2.44	35.59	3.18	134.8	0.137	0.0934	–	–	
S12	2.44	35.59	3.18	134.8	0.137	0.0934	–	–	6
S13	2.44	35.59	3.18	134.8	0.137	0.0934	–	–	7
S14	2.13	53.38	(14.7)	289.1	0.119	0.2296	0.106	0.1297	1
S15	2.13	53.38	(14.7)	321.6	0.119	0.2555	0.106	0.1443	1
S16	2.29	53.38	(13.6)	105.4	0.079	0.0778	0.098	0.1010	1
S17	2.29	62.28	(15.9)	148.3	0.079	0.1096	0.114	0.1405	1
S18	2.29	62.28	(25.9)	140.1	0.079	0.1035	0.114	0.1327	1
S19	2.41	106.76	(8.5)	676.1	0.119	0.4747	0.204	0.2681	1
S20	2.44	35.59	(8.5)	163.2	0.137	0.1132	0.059	0.0482	
S21	2.44	35.59	3.18	119.2	0.137	0.0827	0.059	0.0352	8
L1	0.61	10.32	3.18	11.5	0.079	0.0319	–	–	
L2	1.22	20.64	3.18	14.2	0.079	0.0197	–	–	
L3	1.83	30.96	3.18	22.7	0.079	0.0210	–	–	
L4	2.44	41.28	3.18	27.0	0.079	0.0187	–	–	
L5	2.44+	–	3.18	28.3	0.079	0.0196	–	–	2
L6	2.44+	–	3.18	28.3	0.079	0.0196	–	–	3
L7	2.44	–	3.18	83.2	0.119	0.0577	–	–	3
L8	2.44	–	3.18	83.2	0.119	0.0577	–	–	3
L9	2.44	–	3.18	154.8	0.140	0.1074	–	–	3
L10	2.44	41.28	3.18	176.6	0.168	0.1225	–	–	3
L11	0.61	10.32	3.18	12.9	0.082	0.0358	–	–	
L12	1.22	20.64	3.18	15.6	0.082	0.0216	–	–	
L13	1.83	30.96	3.18	22.7	0.082	0.0210	–	–	

Notes: 1. Thickness corrected by porosity = 0.67.
2. Cover length increased by 0.91 m upstream of frame (0.91×0.61-m sheets).
3. Cover length increased by 1.82 m upstream of frame (0.91×0.61-m sheets).
4. Five blocks removed from downstream screen face in run S8.
5. Ten blocks removed from downstream screen face in run S8.
6. Cover length increased by 0.91 m upstream (single blocks).
7. Cover length increased by 1.82 m upstream (single blocks).
8. Three blocks at 45 to 60° removed from run S20.

vestigate if one can neglect the hydrodynamic force on the leading edge. The data for these experiments can be found in Tables 1 and 2. Both large ice sheets (0.61-x 0.59-m-wide) and ice blocks (all 3.18 mm in thickness) were tested.

From the initial experiment it was determined that a cover length greater than 2 m was necessary to have a proper boundary development and that both the hydrodynamic force at the leading edge and the weight of the ice in the downstream direction can be excluded because of their minor contributions compared to the shear force.

As a check on the sensitivity of the experimental apparatus, smooth flat sheets of 0.16-x 0.59-m-wide polyethylene plastic were placed in the free-swinging frame and the drag force was measured for two flow velocities. In a discussion of the turbulent boundary layer over smooth flat plates, Schlichting (1968) derived the skin friction coefficient based upon the logarithmic velocity distribution and the drag force acting

Table 2. Data taken with velocity profile measurements, $y_t = 0.152$ m.

Run	Length of ice cover L (m)	Weight of cover W (N)	Thickness of cover t (mm)	Total force F_m (mN)	Mean velocity $\bar{V}_m$ (m/s)	Mean ice section velocity $\bar{V}_i$ (m/s)	Shear velocity of ice u_i^* (m/s)	Measured shear stress τ_{im} (N/m²)	Computed shear stress τ_{ic} (N/m²)	Friction factors with V_i f_{ii}	Friction factors with V_m f_{im}	y_m/y_n	t/y_t	Porosity P	t/y_n	Note
V1	2.44	41.28	3.18	76.5	0.130	0.133	0.0122	0.0531	0.149	0.0240	0.0251	0.43	0.021	–	–	1
V2	2.44	41.28	3.18	27.6	0.082	0.078	0.0058	0.0191	0.034	0.0251	0.0227	0.55	0.021	–	–	1
V3	2.44	28.91	3.18	116.1	0.130	0.135	0.0122	0.0805	0.149	0.0353	0.0381	0.53	0.021	–	–	2
V4	1.75	53.38	–	336.7	0.130	–	–	0.3256	–	–	0.1541	–	–	–	0.152	
V5	2.32	71.17	20.4	326.5	0.130	0.104	0.0244	0.2381	0.595	0.1761	0.1127	0.591	0.134	0.71	0.152	
V6	2.23	53.38	26.7	275.3	0.130	0.120	0.0210	0.2089	0.441	0.1161	0.0989	0.563	0.175	0.83	0.123	
V7	2.44	102.31	20.1	516.0	0.130	0.125	0.0212	0.3578	0.449	0.1832	0.1694	0.473	0.132	0.60	0.208	
V8	2.53	102.32	32.8	551.6	0.130	0.131	0.0259	0.3689	0.671	0.1720	0.1746	0.692	0.215	0.62	0.222	
V9	2.44	34.70	3.18	31.5	0.082	0.078	0.0058	0.0218	0.034	0.0287	0.0259	0.550	0.021	–	–	2
V10	2.44	48.93	12.2	94.7	0.082	0.075	0.0085	0.0657	0.072	0.0864	0.0782	0.457	0.080	0.69	0.095	
V11	2.44	71.17	17.5	146.8	0.082	0.078	0.0088	0.1018	0.077	0.1339	0.1211	0.642	0.115	0.68	0.130	
V12	2.44	97.86	20.95	189.0	0.082	0.076	0.0107	0.1311	0.144	0.1816	0.1560	0.718	0.137	0.64	0.181	

Notes: 1. Four large sheets ~ 0.59×0.61 m in frame.
2. Single layer of blocks in frame.

Table 3. Measured and computed drag forces on the smooth ice sheets.

Run	Reynolds number $R_e \times 10^5$	Skin friction coefficient $C_f \times 10^{-3}$	Computed drag force F_c (mN)	Measured drag force F_m (mN)
V1	2.8	5.74	69.9	76.5
V2	1.8	6.37	30.5	27.5

on a plate of zero incidence. However, the Reynolds number for the plate lengths and velocities considered lies in the transition zone, and one must determine whether the boundary layer is laminar, turbulent or in transition over the plate length.

It was initially assumed that the flow was probably turbulent because the ice sheets had blunt square leading edges, thereby tripping the boundary layer into the turbulent regime, and this assumption was later confirmed.

Schlichting (1968) fitted the relation between C_f the coefficient of skin friction and R_e the Reynolds number as developed from the logarithmic velocity profile into a more convenient empirical form for turbulent flows such that

$$C_f = 0.455/(\log_{10} R_e)^{2.58} \qquad (3)$$

where $R_e = (\bar{V}_m L)/\nu$ and ν is the kinematic viscosity.

To compare the measured and calculated values of the total drag acting on a smooth plate, tests V1 and V2 were performed (see Table 2). The drag on the smooth sheets F_c is given by

$$F_c = \tfrac{1}{2}\rho_f C_f \bar{V}_m^2 BL. \qquad (4)$$

Table 3 gives the measured drag force and the computed values for these two test runs.

The measured values of the drag force are in relatively close agreement with those values obtained using the Prandtl-Schlicting turbulent flow relationship for the skin friction. Based on this information, it was concluded that the apparatus was capable of measuring quite accurately the shear stress exerted by the fluid to a floating cover and that the boundary layer was in fact turbulent.

The effect of ice cover length in the frame on the drag force measured is indirectly shown in Figure 2. For the low velocity tests with short cover lengths the measured forces are extremely low (< 15 mN), and the effect of the hydrodynamic force and weight of the ice cover becomes increasingly important with

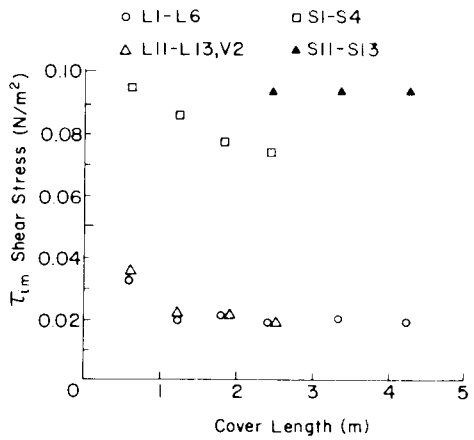

Figure 2. The decreasing effect of the leading edge form drag with increasing cover length as measured by the overall shear stress.

decreasing length. For example, L1 with a cover length of 0.61 mN has a potential contribution from the hydrodynamic force of roughly 6 mN, using C_d = 0.1. Consequently, short cover lengths would give higher values of shear stress if the hydrodynamic force were not subtracted, and this is shown in Figure 2. The value of the effective shear stress decreases with increasing cover length for tests L1 and L2 but remains nearly constant for L3-L6.

For runs L5 and L6, additional sheets were placed immediately upstream of the frame, such that a proper boundary layer and velocity distribution might be achieved. These additional sheets did not come in contact with the suspended frame, and for the low velocity flow under the large sheets, the shear stress was nearly constant after the cover had reached a length of roughly 2 m. In experiments S11-S13 (small blocks of one layer thickness), the cover was extended upstream from the frame approximately 0.9 and 1.8 m respectively, and again a constant value of shear stress was maintained. The data for the higher velocity flows (S1-S4 and S11-S13) seem to suggest that a cover length of approximately 2.4 m was satisfactory for measuring the shear stress and the effects of the hydrodynamic force are now small compared to the shear force.

The velocity profiles at 0.76 m from the downstream end of the frame are shown in Figure 3 for increasing cover lengths upstream. These profiles reveal that, at higher velocities (~0.13 m/s), a cover length of 2.5 to 3.5 m is necessary for proper boundary layer development at the velocity measuring position.

A relative minimum thickness of the ice jam can be computed on the basis of the surface area of ice in the frame and the total weight introduced upstream. This

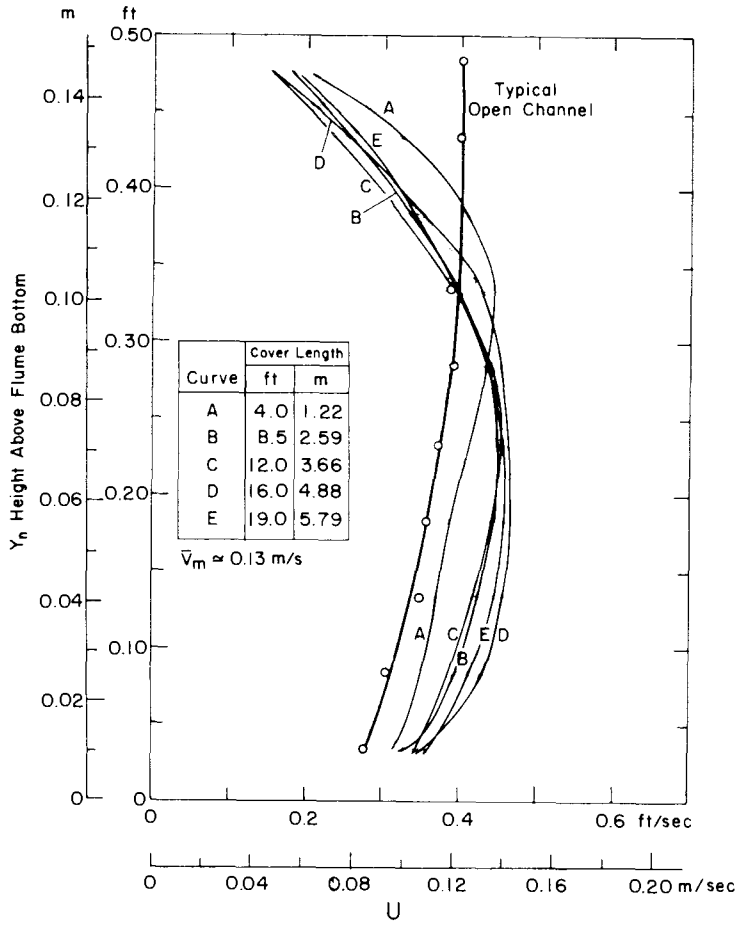

Figure 3. Velocity profiles at 0.76 m from the downstream end for increasing cover lengths upstream.

would represent the minimum thickness obtainable with no allowance for porosity. It will be shown that the porosity remains relatively constant for all tests. The absolute roughness on the underside of the accumulated ice was not measured because time did not permit extensive measurements during these tests.

The orientation of the blocks in the ice cover at the downstream end of the frame had a significant effect on the total force measured. For example, run S20 had three blocks against the downstream wire screen at 45°–60°; removing only these three blocks resulted in a 27% decrease in the force exerted on the system as measured in run S21. This same observation was noted in run S8, where five blocks were removed at the wire screen for run S9 and five more for run S10, effecting a 30% reduction in total force from run S8.

For run S20, the computed drag force

$$F_a = (\rho V^2 A C_d)/2 \qquad (5)$$

on these three blocks at 60° is approximately 30 mN (where $C_d = 1.0$ and A is the projected area of the block). Comparison of this value with the loss in force of 44 mN measured by the system when the blocks were removed indicates that a few blocks can account for a major portion of the force due to large areal projections. These two observations clearly show that care must be taken at the downstream end so that unobstructed ice floes do not project excessively into the flow at steep angles and create excessive drag forces compared to the skim drag of the accumulation thickness.

For short ice cover lengths ($L/B < 3.0$), the hydrodynamic drag F_H appears to be an important contributor, but as the cover length increases, the ratio of the hydrodynamic form drag on the leading edge to the total load is small (< 0.05). This is because the ice cover underside drag force is significantly greater than the ice cover frontal form drag.

The velocity profiles beneath the simulated ice covers are quite similar except that the roughness of the respective boundaries influences the position of the maximum velocity. Figure 4 shows the velocity

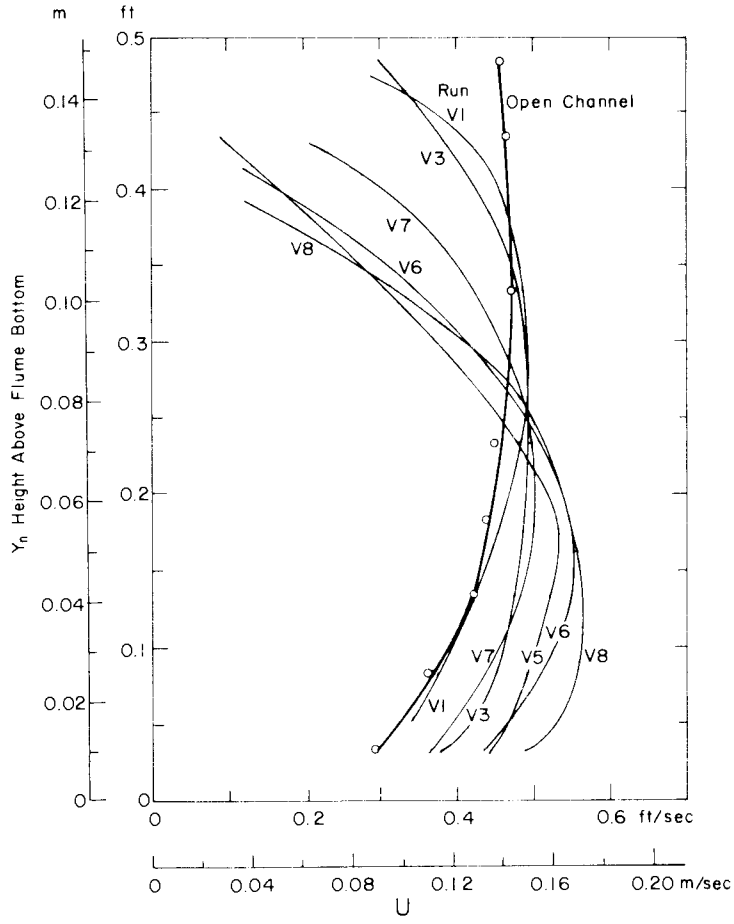

Figure 4. Velocity profiles at 0.76 m from downstream end beneath rough ice covers.

profiles and the corresponding change in position of the maximum velocity due to both increasing cover thickness and boundary roughness. Because the flume bottom was relatively smooth, the position of maximum velocity with the large ice sheets was nearly one-half the depth of flow beneath the cover. As the cover increased in roughness (created by introducing greater quantities of ice blocks per unit time upstream), the position of maximum velocity approached the smoother boundary.

ANALYSIS OF DATA

The data in Tables 1 and 2 represent the results of the shear stress measurements on single thickness large sheets (L), small blocks (S) and on both the sheets and blocks when the velocity profile measurements were taken (V).

$\overline{V}_i$ is the mean velocity of the flow beneath the ice cover in the region from the point of maximum velocity to the bottom of the ice cover as determined from the velocity profiles. The shear velocity in the ice section u_i^* was determined from the velocity profiles, assuming a logarithmic velocity distribution from the ice bottom to the point of maximum velocity.

The biggest difficulty in calculating the shear stress lies in assessing the position of zero velocity with respect to the boundary of the underside of the ice cover. Since the boundary is very irregular, it is extremely difficult to locate from measurements. Furthermore, a question arises as to where one should take the velocity profile measurements. Hence, the calculation of the friction velocity from the velocity profiles is critical, as the position of the boundary can significantly influence the slope of the velocity profile gradient. The shear stress computed from the relation $\tau_{ic} = u_i^{*2}\rho_f$ uses the friction velocity u_i^* as calculated from the velocity profile gradient.

The general equation for Darcy's coefficient of friction f is

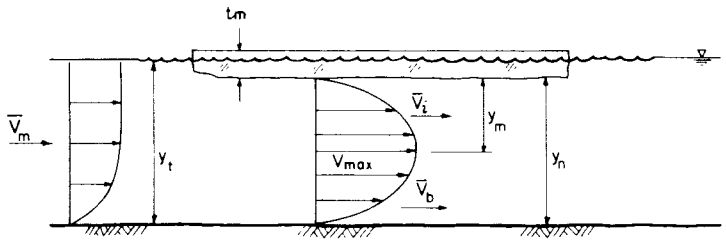

Figure 5. Definition sketch of flow symbols.

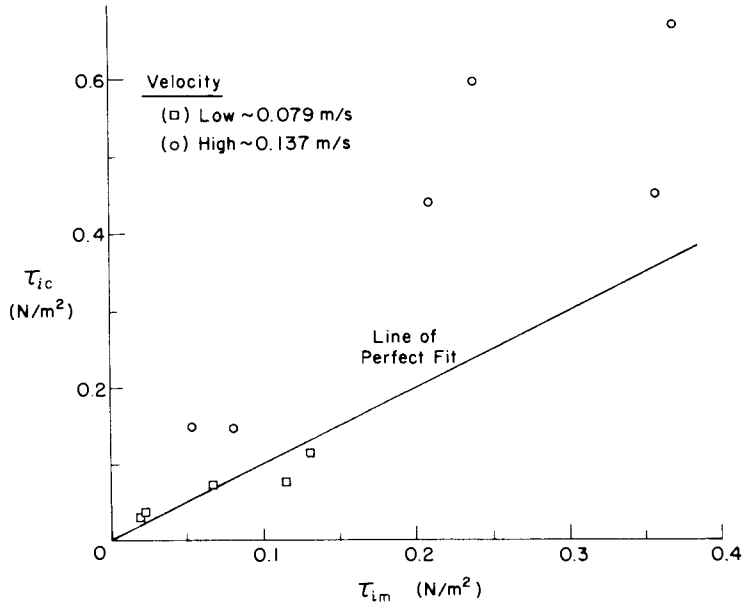

Figure 6. Relationship between computed and measured values of the ice cover shear stress.

$$f = 8\tau/\rho_f V^2. \qquad (6)$$

The specific resistances f_{ii} are calculated using the mean velocity in the ice section $\overline{V}_i$, and f_m is the calculated friction coefficient using the mean channel velocity $\overline{V}_m$ (see Fig. 5 for illustration of terms).

The porosity ρ of the ice accumulation was calculated from the data contained in Table 2. The ice cover porosity is defined as the ratio of the volume of the voids filled with water to the total volume. The porosity values are consistent with those obtained by Tatinclaux and Cheng (1978).

Figure 6 shows the comparison of the shear stress calculated from eq 2 and that computed from the velocity profile reduction. For the low velocity runs (0.082 m/s) the agreement between the measured and calculated shear stress was adequate, but the higher velocity tests showed an increasing divergence of almost 2:1 for computed vs measured values.

Several investigations have shown that the logarithmic distribution fails to conform to the observed velocity profile when large discrete roughness elements are present at the boundary (Davar and Ismail 1977, O'Laughlin 1965, and Ismail 1977). Although the logarithmic velocity equation appeared to be a reasonable fit of the velocity profile, the von Karman constant k (i.e. the ratio of friction velocity and the logarithmic gradient of the mean velocity) seems to vary.

There are four possible explanations for the discrepancy in the shear stress data at the higher velocity tests:

1. The propeller current is not small compared to the flow depth.
2. The propeller many not be responding properly to shear flow.
3. The porous boundary may be important and three dimensional flow may be present.
4. The exact position of the zero velocity near the

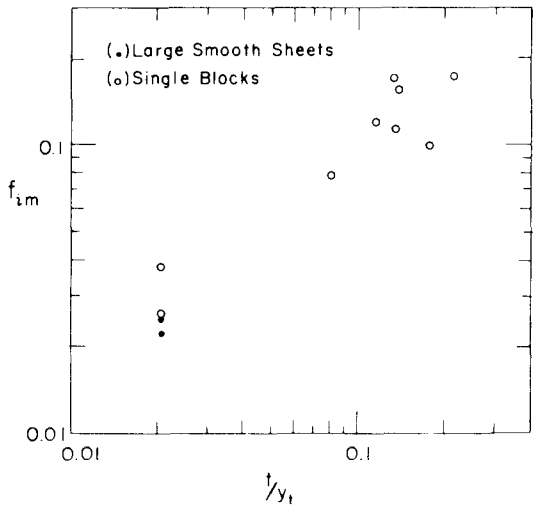

Figure 7. Typical friction factor relationship with normalized ice cover thickness using V_m.

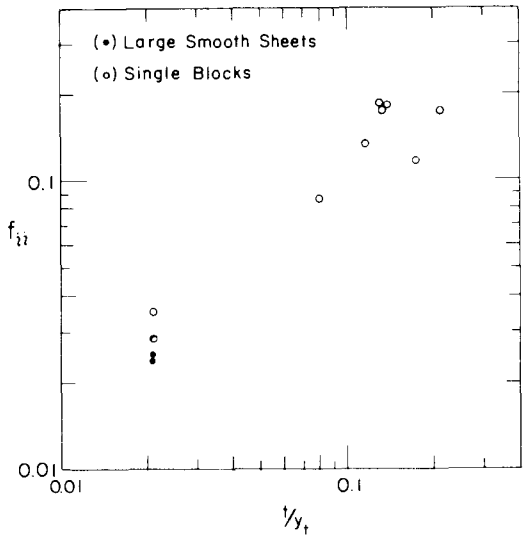

Figure 8. Typical friction coefficient relationship with normalized ice cover thickness using $\overline{V}_i$.

porous boundary is in question; Chu and Gelhar (1972) obtained a von Karman constant of 0.27 above a porous wall.

Sufficient information was obtained to calculate the coefficient of friction factor f for the tests based on the frame force measurements. Two values of the friction factor were calculated for runs V1-V12, one using the mean upstream open water flow velocity $\overline{V}_m$ and the second the mean velocity of the flow in the ice region $\overline{V}_i$.

Normalizing the measured thickness by the upstream depth, two plots of f_{im} and f_{ii} vs t/y_i are presented (Fig. 7 and 8), which generally confirm the assumption that the roughness of the cover increases with increasing cover thickness. The mean velocity in the ice section was usually lower than the upstream open flow mean velocity which leads to slightly higher friction factors.

Earlier data were collected on the ice cover shear stress where the thickness of the cover was not measured, and an attempt was made to recover the estimated thickness. In runs V5-V12, excluding V9, the porosity of the accumulation can be calculated from measurements of the average ice thickness and volume of ice in the test. Taking the average porosity value of $p = 0.67$, the expected thickness is shown in parentheses in Table 1.

On the assumption that the roughness increases in proportion to the ice cover thickness for these data, the friction factor f_{im} can be plotted vs the nondimensional roughness parameter t/y_n as is shown in Figure 9. Using all the data from Tables 1 and 2 with accumulation lengths greater than 2 m and with more than a single thickness ice cover, it can be seen that the data lie within the same general zone as that shown by Tatinclaux and Cheng (1978). A regression fit on the new data was omitted because they appear to fall within the same general range as those of previous investigators, although maybe slightly lower.

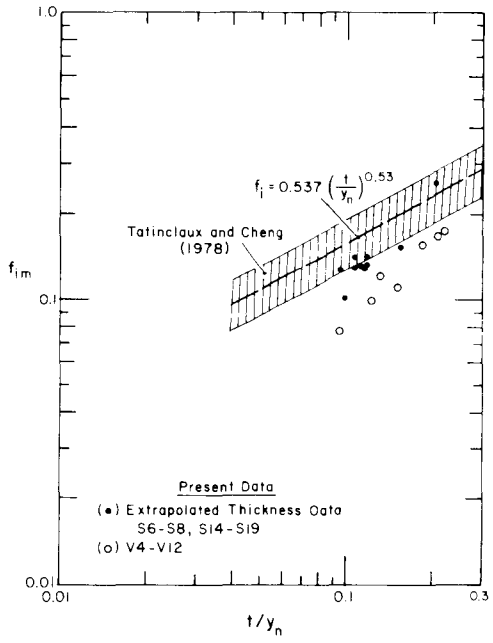

Figure 9. Relationship between Darcy's f and the normalized ice cover thickness compared with Tatinclaux and Cheng's 1978 data points which are represented by a shaded area containing 90% of their data.

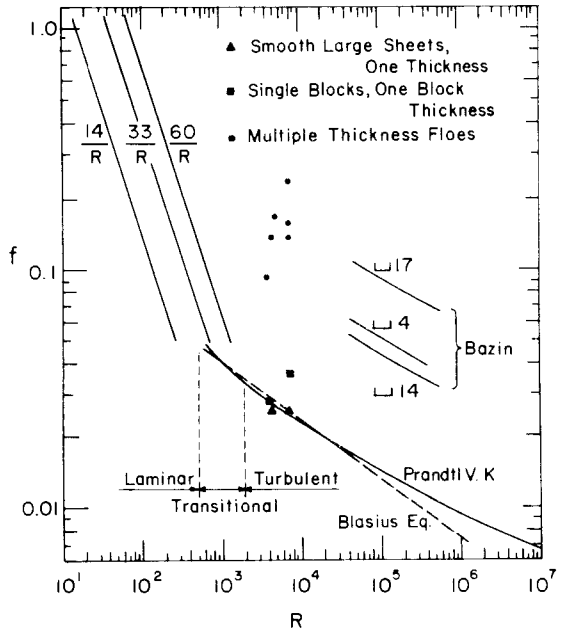

Figure 10. The friction factor–Reynolds number relationship for open channels with different flow regimes (see Chow 1959).

The assumption that the roughness of the underside of the fragmented ice cover increases with the cover thickness is not a strong indicator of the roughness but appears adequate for this single block size experiment. For all future experiments, the roughness heights should be measured and used in place of the ice cover thickness, and field measurements of ice jam roughness elements would be extremely valuable to guide further work.

The friction factor for the various types of ice cover—1) large sheets 2) single thickness blocks and 3) multiple thickness covers—are plotted vs the Reynolds number $R_l = \overline{V}_l l/\nu$, where l is a characteristic length chosen to be the hydraulic radius R in Figure 10 (from Chow 1959).

The data for the large smooth sheets lie near the Blasius equation for turbulent flow over flat plates, while a cover of a single thickness of small blocks shows a slightly higher resistance. The scatter in the multiple floe thickness data lies in the regions of the various Bazin channels.

Nezhikhovskiy (1964) presented data on the Mannings roughness coefficient n and thickness of ice sheets for rivers. His data points are replotted in Figure 11 along with the laboratory data of this study. Both sets of data follow the general trend of increasing roughness coefficients for greater ice block thicknesses. It is clear that the two data sets are in different regimes, but the roughness coefficients increase at nearly the same exponential rate of 0.4.

CONCLUSIONS

The method presented for measuring the shear stress on the underside of fragmented covers in small-width channels eliminates the effect of wall friction force which is significant. The shear stress computed from the velocity profiles for the higher velocity experiments was on the order of twice the measured values, indicating a deficiency in the von Karman-Prandtl logarithmic velocity distribution. This effect may stem from 1) inability to adjust the profile to the boundary where the velocity is zero, 2) three-dimensional flows around the large roughness elements, or 3) the possibility of the porous wall influence.

The nondimensional friction factor f based on the thickness of the fragmented ice cover was adequate in assessing the roughness, indicating that the roughness was proportional to the increasing thickness of the cover. The values for the friction coefficient of the model ice are in agreement with various reported values for real ice covers (Carey 1966, 1967, Tesaker 1970, Nezhikhovskiy 1964).

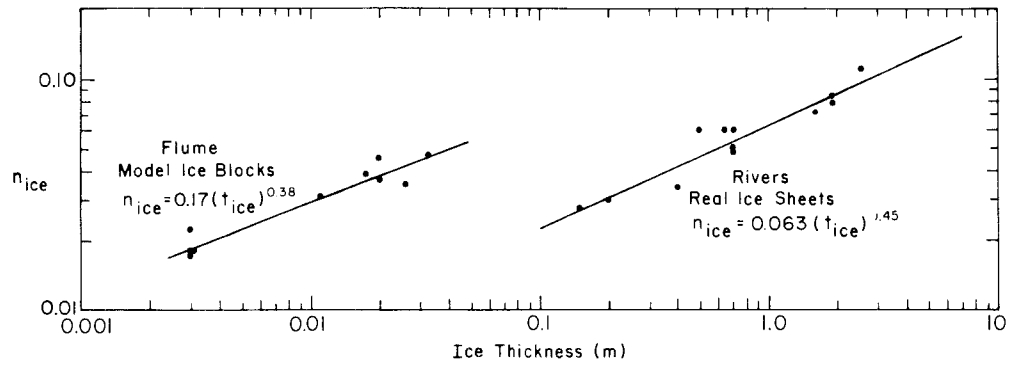

Figure 11. Empirical relationship between roughness coefficient and thickness of the ice cover.

LITERATURE CITED

Ashton, G.D., M.S. Uzuner and J.F. Kennedy (1970) Two investigations of river ice. Iowa Institute of Hydraulic Research Report 129.

Carey, K. (1966) Observed configuration and computed roughness of the underside of river ice, St. Croix River, Wisconsin. U.S. Geological Survey Professional Paper 550-B, p. B192-B198.

Carey, K.L. (1967) The underside of river ice, St. Croix River, Wisconsin. U.S. Geological Survey Professional Paper 575-C, p. C195-C199.

Chow, V.T. (1959) *Open channel hydraulics.* New York: McGraw-Hill.

Chu, Y.H. and Gelhar, L.W. (1972) Turbulent pipe flow with granular permeable boundaries. Report 148, Ralph M. Parson Laboratory, Massachusetts Institute of Technology.

Davar, K.S. and E. Ismail (1977) Effects of large roughness on resistance and dispersion in channels. *Proceedings of Third National Hydotechnical Conference*, University of Leval, Quebec, P.Q., Canada, p. 453-482.

Ismail, E. (1972) Resistance to flow in rectangle conduits with unsymmetrical roughness. M.S. thesis (unpublished), Dept. of Civil Engineering, University of New Brunswick, Fedricton, N.B., Canada.

Nezhikhovskiy, R.A. (1964) Coefficients of roughness of bottom surface of slush-ice cover. *Soviet Hydrology: Selected Papers*, no. 2, American Geophysical Union.

O'Laughlin, E.M. (1965) Resistance to flow over boundaries with small roughness concentrations. Ph. D. thesis (unpublished) submitted to Mechanics and Hydraulic Department, University of Iowa.

Ohashi, K., and T. Hanada (1970) Flow measurements of ice covered rivers in Hokkaido. *International Association of Hydraulic Research Symposium: Ice and Its Action on Hydraulic Structures.* Reykjavik, paper 1.4.

Pariset, E., and R. Hausser (1961) Formation and evolution of ice covers on rivers. *Transactions of the Engineering Institute of Canada*, vol. 5, no. 1, p. 41-49.

Schlichting, D. (1968) *Boundary layer theory.* 4th ed. New York: McGraw-Hill Book Company.

Tatinclaux, J.C., C.L. Lee, T.P. Wang, T. Nakato and J.F. Kennedy (1977) A laboratory investigation of the mechanics and hydraulics of ice jams. CRREL Report 77-9. AD A032471.

Tatinclaux, J.C. and S. Cheng (1978) Characteristics of river ice jams. *Proceedings, International Association of Hydraulic Research Symposium–Ice Problems*, Lulea, Sweden, vol. 2, p. 463-475.

Tesaker, E. (1970) Measurements of ice roughness and the effect of ice cover on water levels in three Norwegian rivers. *International Association of Hydraulic Research Symposium: Ice and Its Action on Hydraulic Structures.* Reykjavik, paper 3.4.